

Enhancing the Josephson diode effect with Majorana bound states

Jorge Cayao,¹ Naoto Nagaosa,² and Yukio Tanaka³

¹*Department of Physics and Astronomy, Uppsala University, Box 516, S-751 20 Uppsala, Sweden*

²*Center for Emergent Matter Science (CEMS), RIKEN, Wako, Saitama, 351-0198, Japan*

³*Department of Applied Physics, Nagoya University, Nagoya 464-8603, Japan*

(Dated: September 28, 2023)

We consider phase-biased Josephson junctions with spin-orbit coupling under external magnetic fields and study the emergence of the Josephson diode effect in the presence of Majorana bound states. We show that junctions having middle regions with Zeeman fields along the spin-orbit axis develop a low-energy Andreev spectrum that is asymmetric with respect to the superconducting phase difference $\phi = \pi$, which is strongly influenced by Majorana bound states in the topological phase. This asymmetric Andreev spectrum gives rise to anomalous current-phase curves and critical currents that are different for positive and negative supercurrents, thus signaling the emergence of the Josephson diode effect. While this effect exists even without Majorana states, it gets enhanced in the topological phase as Majorana bound states become truly zero modes. Our work thus establishes the utilization of topological superconductivity for enhancing the functionalities of Josephson diodes.

Diodes represent a class of devices that conduct current primarily along one direction and are key building blocks of numerous electronic components [1–6]. Diodes have been initially studied in the normal state [7–9], where inevitable energy losses appear due to finite resistance. To overcome this issue, superconductors have been recently proposed to host superior diode functionalities [10–12], with dissipationless supercurrents in bulk systems [13–17] and in Josephson junctions (JJs) [18–21]. Of particular interest are diodes in JJs, also known as Josephson diodes (JDs), because supercurrents here are controllable by virtue of the Josephson effect, which arises due to the finite phase difference between coupled superconductors [22, 23]. The finite phase difference also enables the formation of Andreev bound states (ABSs), shown to determine the profile of supercurrents [24–34] and reveal the nature of emergent superconductivity [35–46].

The majority of studies on JDs have involved systems with spin-orbit coupling (SOC) and magnetic fields, with experiments that strongly support their realization in semiconductor-superconductor junctions [14, 19, 47]. Moreover, JDs are characterized based on their quality factors (efficiency), which measure the diode’s ability to conduct current along one direction and, in JJs, it implies different critical currents along opposite directions. In this regard, recent works have reported sizeable and highly tunable quality factors, showing that JJs with SOC and magnetism hold great promise for JDs.

Superconductors with SOC under magnetic fields have also been explored for realizing topological superconductivity [35, 43–46, 48–52], a topological state of matter that hosts Majorana bound states (MBSs) and promises to revolutionize future quantum technologies. MBSs emerge above a critical magnetic field as charge-neutral topologically protected quasiparticles and exhibit spatial nonlocality [53–57], properties that have been recently explored in JJs [58–65] and shown to provide a solid way for topological qubits [66–70]. While the detection

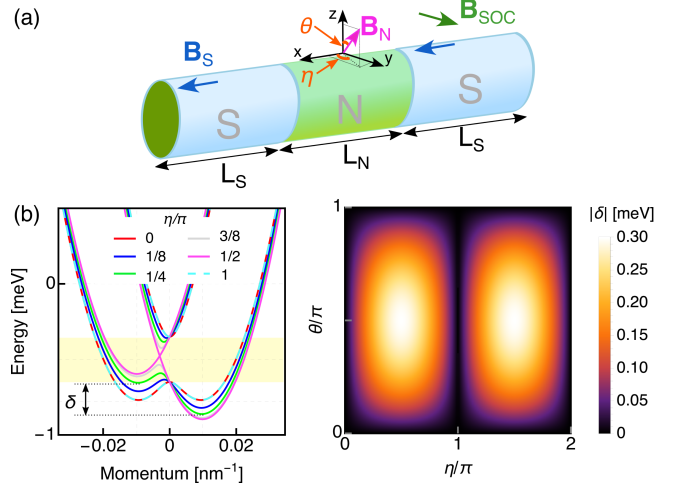


FIG. 1. (a) A JJ based on a nanowire with SOC field \mathbf{B}_{SOC} along y -axis (green), where the normal (N) and superconducting (S) regions have length L_N and L_S . The N region has a Zeeman field \mathbf{B}_N (magenta arrow) with components perpendicular and parallel to \mathbf{B}_{SOC} ; the S regions have a Zeeman field \mathbf{B}_S that is only perpendicular to \mathbf{B}_{SOC} . (b) Energy versus momentum without superconductivity: while a perpendicular Zeeman field opens a gap at zero momentum (yellow region), a parallel Zeeman term induces an asymmetry in the bands, δ , seen by fixing the angle of \mathbf{B}_N with the z -axis to $\theta = \pi/2$ and varying the angle from the x -axis η . The solid red ($\eta = 0$) and dashed cyan curves ($\eta = \pi$) are superimposed. Left panel shows δ at $\eta = \pi/4$ (green curve). Right panel: δ at the SOC momenta as function of θ and η . Parameters: $B_N = 0.15\text{meV}$, $\alpha = 40\text{meVnm}$, $\mu = 0.5\text{meV}$.

of MBSs has recently attracted a lot of interest [43–46], the realization of JDs in topological superconductors and their responses due to the presence of MBSs has received very limited attention so far [71–75]. In particular, it is still unknown how JDs respond to the Majorana nonlocality, an open question that could establish the realization and use of JDs for topological quantum phenomena.

In this work we consider superconductor-normal-superconductor (SNS) JJs with SOC and Zeeman fields, and discover the emergence of highly tunable JDs, which acquire quality factors that can be greatly enhanced by MBSs, specially, when they become more nonlocal. We find that these topological JDs occur when the middle N region has a Zeeman field with a component that is parallel to the SOC, a regime that exhibits an asymmetric phase-dependent Andreev spectrum which then gives rise to supercurrents and critical currents with non-reciprocal behaviour defining the JDs. While JDs can occur even when the JJ is trivial, it is only in the topological phase that the supercurrents and quality factors exhibit a strong dependence on the Majorana nonlocality, thus establishing the potential of MBSs for designing JDs with topologically protected and enhanced properties.

JJs based on nanowires.—We consider SNS JJs formed on a single channel nanowire with Rashba SOC [Fig. 1(a)], with a continuum model given by

$$H = \xi_{p_x} \tau_z + \frac{\alpha}{\hbar} p_x \sigma_y \tau_z + \Delta(x) \sigma_y \tau_y + H_Z(x), \quad (1)$$

where $\xi_{p_x} = p_x^2/(2m) - \mu$ is the kinetic part, $p_x = -i\hbar\partial_x$ is the momentum operator, μ is the chemical potential, α is the Rashba SOC strength, $H_Z(x)$ is the space dependent Zeeman field, $\Delta(x)$ the induced space dependent s -wave pair potential, and σ_i and τ_i are the i -th Pauli matrices in spin and electron-hole spaces, respectively. For computational purposes, the continuum Hamiltonian in Eq. (1) is discretized into a tight-binding lattice with spacing $a = 10$ nm and then divided into three regions (left/right S and middle N) of finite lengths $L_{S,N}$ [62, 65], see Fig. 1(a). The S regions have a finite pair potential Δ with a finite phase difference ϕ , while N has $\Delta = 0$, originating a finite SNS JJ. The Zeeman field is considered to have a different structure in N and S regions $H_Z(x) = \mathbf{B}_{S(N)} \cdot \boldsymbol{\Sigma}$ with and $\boldsymbol{\Sigma} = (\sigma_x \tau_z, \sigma_y, \sigma_z \tau_z)$, with the aim to ensure that JD effect and MBSs can coexist. Thus, the Zeeman field in the S regions is taken along x axis, $\mathbf{B}_S = (B, 0, 0)$, while along all directions in N as $\mathbf{B}_N = B_N(\sin\theta \cos\eta, \sin\theta \sin\eta, \cos\theta)$, with $\theta \in (0, \pi)$ and $\eta \in (0, 2\pi)$. Moreover, we consider realistic system parameters, with $\alpha_R = 40$ meVnm and $\Delta = 0.5$ meV, which are in the range of experimental values reported for InSb and InAs nanowires, and Nb and Al superconductors [43].

Before going further, we stress that the role of the Zeeman field can be already seen in the normal state, by inspecting the bands of Eq. (1) with $\Delta = 0$ and \mathbf{B}_N . While a component of \mathbf{B}_N perpendicular to the SOC opens a gap at zero momentum $k = 0$ (yellow region), the band dispersion becomes asymmetric with respect to $k = 0$ when \mathbf{B}_N has a parallel component to such SOC, see left panel of Fig. 1(b). This asymmetry can be characterized by the difference between the lowest bands at the SOC momenta $\pm m\alpha/\hbar^2$, denoted by δ , which acquires a maximum at $\theta = \eta = \pi/2$ [Fig. 1(b)]. Below

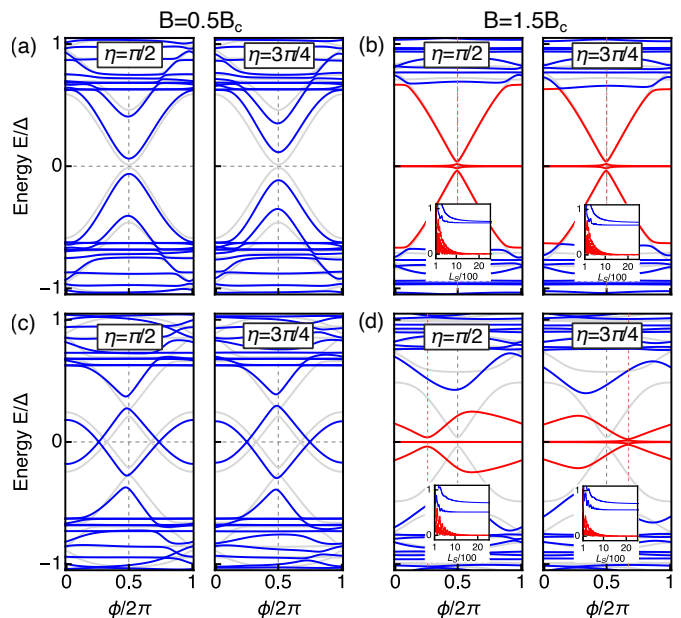


FIG. 2. Low-energy spectrum of JJs with $L_N = 20$ nm (a,b) and $L_N = 100$ nm (c,d) as a function of ϕ for $B < B_c$ and $B > B_c$ at different η . In (b,d) the nearest levels to zero are depicted in red color, while insets show the lowest four positive levels as a function of L_S . Vertical dashed lines mark where four MBSs appear. Gray curves in all panels correspond to $\eta = 0$. Parameters: $\alpha = 40$ meVnm, $\mu = 0.5$ meV, $\theta = \pi/2$, $L_S = 1000$ nm, $\Delta = 0.5$ meV, $B_N = 0.5$ meV.

we will see that this asymmetry is crucial for achieving non-reciprocal Andreev spectrum and JDs in JJs.

Non-reciprocal phase-dependent Andreev spectrum.—To start, we focus on the Andreev spectrum, which is presented in Fig. 2 as a function of ϕ for JJs with $L_N = 20$ nm and $L_N = 100$ nm at distinct η and B . The first observation is that the Andreev spectrum strongly depends on ϕ , revealing the appearance of ABSs within the induced gap, with interesting dependences on η , L_N , and B . At $\eta = 0$, i.e., when the Zeeman field in N is perpendicular to the SOC, the spectrum is symmetric with respect to $\phi = \pi$, see gray curves in Fig. 2. Here, for $B = B_c$, with $B_c = \sqrt{\mu^2 + \Delta^2}$, defines a topological phase transition into a topological phase ($B > B_c$) with four topological ABSs that depend on ϕ [58, 61, 76]. Correspondingly, for $B < B_c$ the system is in the trivial phase and hosts two pairs of conventional spin-split ABSs having a cosine-like dependence on ϕ [27, 33]. The topological ABSs at $\phi = \pi$ define four MBSs, two at the outer sides of S and two at their inner sides, while the ABSs at $\phi = 0$ only two MBSs located at two outer sides of the S regions [58, 61, 76]. For JJs with short S regions, the four MBSs split around zero energy at $\phi = \pi$, thus giving rise to a Majorana zero-energy splitting, which gets considerably suppressed for long S regions and can be thus seen as a signal of the Majorana spatial nonlocality [63, 65].

When the Zeeman field \mathbf{B}_N in N acquires a compo-

ment that is parallel to the SOC, characterized here by $\eta \neq 0$, the low-energy spectrum becomes highly asymmetric with respect to $\phi = \pi$ and develops important differences from the $\eta = 0$ case in both the topological and trivial phases [Fig. 2(c,d)]. The asymmetry is reflected in the ingap ABSs, which involve MBSs in the topological phase, and also in the quasicontinuum above the induced gap. For JJs with $L_N = 20\text{nm}$ and $\eta \neq 0$ exists only a small asymmetry with respect to $\phi = \pi$ in the quasicontinuum but no substantial effect is seen by naked eye at low energies [Fig. 2(a,b)]; by zooming in, it is possible to see that a very tiny asymmetry at low-energy around $\phi = \pi$. Note that the Majorana zero-energy splitting gets suppressed as L_S increases, consistent with their inherent spatial nonlocality, see red curves in insets of Fig. 2(b); the ABSs for $B < B_c$ do not depend on L_S . In JJs with $L_N = 100\text{nm}$ the Andreev spectrum exhibits a stronger response to $\eta \neq 0$ [Fig. 2(c,d)]. While the trivial spectrum here is only weakly asymmetric [Fig. 2(c)], we verified that JJs with other values of L_N have spectra with larger asymmetries [77], see Supplementary Material (SM) [78]. Irrespective of L_N , however, the asymmetric trivial Andreev spectrum does not depend on L_S because the ABSs here are located only at the inner side of the JJ. In contrast, the Andreev spectrum for $B > B_c$ is more noticeable and strongly depends on L_S due to the presence of MBSs. In particular, the Majorana zero-energy splitting can occur at ϕ other than $\phi = \pi$ when $\eta \neq 0$ [Fig. 2(d)], thus showing the key role of \mathbf{B}_N for inducing an asymmetric Andreev spectrum in topological JJs. Since the Majorana zero-energy splitting depends on L_S and $\eta \neq 0$, longer S regions give rise to four MBSs with zero energy which then produce sharper zero-energy crossings that are asymmetric with respect to $\phi = \pi$ as a unique effect due to MBSs, see insets in Fig. 2(d). As a result, finite topological JJs host a nonreciprocal length dependent Andreev spectrum entirely due to MBSs.

Nonreciprocal current-phase curves.—Having established that the Andreev spectrum of JJs under Zeeman fields parallel to the SOC is asymmetric with respect to $\phi = \pi$, here we study how this asymmetry affects the supercurrents $I(\phi)$. At zero temperature, we obtain $I(\phi)$ as [27, 61] $I(\phi) = -(e/\hbar) \sum_{\varepsilon_n > 0} [d\varepsilon_n(\phi)/d\phi]$, where $\varepsilon_n(\phi)$ are the phase-dependent energy levels found in the previous section which include the contribution of both the ingap ABSs and the discrete quasicontinuum [62, 63]. In Fig. 3(a-c) we present $I(\phi)$ for JJs with $L_N = 100\text{nm}$ as a function of ϕ for different η and L_S in the trivial ($B < B_c$) and topological ($B > B_c$) phases. To better understand the role of MBSs, panel (d) shows the contribution of MBSs (I_{MBS}) and the rest of levels (I_{rest}) to the total $I(\phi)$ for L_S ; note that I_{rest} includes the contribution due to the additional ingap ABSs that coexist with MBSs and also of the quasicontinuum.

The first observation in Fig. 3(b,c) is that $I(\phi)$ has an overall asymmetric profile with respect to $\phi = \pi$ at $\eta \neq 0$,

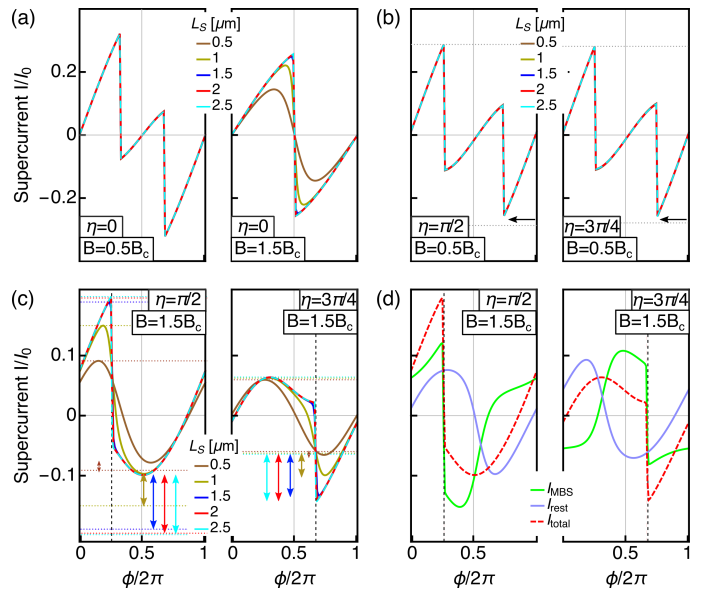


FIG. 3. (a) Supercurrents $I(\phi)$ in JJs with $L_N = 100\text{nm}$ as a function of ϕ at $\eta = 0$ for $B < B_c$ and $B > B_c$ and different L_S . (b,c) same as (a) but at $\eta = \pi/2, 3\pi/4$. Horizontal dotted lines mark $\pm I_c^\pm$; arrows in (b,d) indicate that $I_c^+ \neq I_c^-$. (d) Contributions of the four MBSs and the rest of levels (ABSs and quasicontinuum) to the total $I(\phi)$ for $L_S = 2\mu\text{m}$. Parameters: $I_0 = e\Delta/\hbar$ and the rest as in Fig. 2.

with the asymmetry depending on η and B , and, importantly, with a distinct response in the trivial (topological) phase to changes in L_S . This asymmetric $I(\phi)$ at $\eta \neq 0$ is different to what is found at $\eta = 0$ [Fig. 3(a)], see also [61, 76, 79]. The weak (strong) asymmetry in $I(\phi)$ with respect to $\phi = \pi$ stems from the phase-dependent Andreev spectrum obtained in Fig. 2, which already suggests an important role of the ingap ABSs and quasicontinuum. The trivial phase shows a weak asymmetry for the chosen L_N due to the weakly asymmetric spectrum, but we have verified that other values give far more asymmetric $I(\phi)$. As a result of the asymmetry, $I(\phi)$ develops a global maximum that is distinct to its global minimum, namely, different critical currents $I_c^+ \neq I_c^-$, where $I_c^\pm = \max_\phi[\pm I(\phi)]$, see black arrow in Fig. 3(b). Furthermore, an interesting property of this trivial phase is that $I(\phi)$ does not change when L_S increases for any η . This insensitivity originates from that the ABSs for $B < B_c$ emerge located at the inner sides of the JJ and thus do not depend on L_S , i.e., trivial ABSs are not spatially nonlocal.

In contrast to $B < B_c$, in the topological phase, $I(\phi)$ develops a larger asymmetry with respect to $\phi = \pi$ and sizeable finite values at zero phase [80], which can be traced back to the Andreev spectrum Fig. 2(d). Interestingly, the asymmetry of $I(\phi)$ and $I_c^+ \neq I_c^-$ strongly depend on L_S , which is due to the presence of MBSs and different to what occurs in the trivial regime. To see supercurrents with $I_c^+ \neq I_c^-$ we have indicated

with colored arrows the remaining difference between the two critical currents Fig. 3(c); we note that $I_c^+ = I_c^-$ for $\eta = 0$, as expected [Fig. 3(a)]. Interestingly, the regimes with $I_c^+ \neq I_c^-$ signal the emergence of non-reciprocal supercurrents, also known as the Josephson diode effect (JD effect), which here occurs in the trivial and, notably, also in the topological phases. While JDs in semiconductor-superconductors have already reported before, their emergence in topological JJs is intriguing because MBSs are naturally present in this regime. The effect of MBSs is evident by noting the strong dependence of $I_c^+ \neq I_c^-$ on L_S pointed out above. In fact, the topological phase hosts four spatially nonlocal MBSs exhibiting a zero-energy splitting at $\phi = \pi$ at $\eta = 0$ or away from π when $\eta \neq 0$ [Fig. 2(d)]. Then, by reducing the zero-energy Majorana splitting with increasing L_S , the current-phase curves acquire sharper sawtooth profiles, with larger differences between I_c^+ and I_c^- that can be easily distinguished from the trivial regime. The role of MBSs can be further seen in the individual contributions of the four MBSs and the rest of levels to the total supercurrent $I(\phi)$ in Fig. 3(d). While I_{rest} has a sizeable phase dependent value, the sharpness in the sawtooth profile of $I(\phi)$ (vertical dashed black line) is largely determined by the contribution of MBSs due to the reduction in the Majorana zero-energy splitting for large L_S . These results therefore demonstrate that MBSs play a key role for enhancing the JD effect in the topological phase.

Critical currents and quality factors.—To further understand and characterize the JDs found in previous section, here we present the critical currents I_c^+ and I_c^- and the associated quality factors $Q = |I_c^+ - I_c^-| / (I_c^+ + I_c^-)$. Having $Q \neq 0$ reveals the amount of nonreciprocity in the critical currents and a finite JD effect. In Fig. 4(a-d) we show I_c^\pm as a function of B for $\eta = \pi/2, 3\pi/4$ and distinct L_S , while in Fig. 4(e-h) we present the corresponding Q as a function of B . To contrast, we also show the critical currents at $\eta = 0$ in black-yellow curves of Fig. 4(a-d). The immediate feature we notice is that $\eta \neq 0$ gives rise to $I_c^+ \neq I_c^-$, depicted by the orange colored regions, thus highlighting the realization of JDs. We see that the JD requires a finite B in both cases $\eta = \pi/2, 3\pi/4$ for the chosen L_N but in the SM show that it can already appear at $B = 0$ [78]. Both critical currents I_c^\pm reduce as B increases but $I_c^+ \neq I_c^-$ persists and develop a kink at $B = B_c$, followed by finite current values for $B > B_c$, see Fig. 4(a,b) [81]. Increasing L_S does not change the difference between critical currents I_c^\pm in the trivial phase, but, interestingly, it does in the topological phase which suggests a larger nonreciprocity and the realization of an enhanced JDs [Fig. 4(c,d)]. As exposed in previous sections, the sensitivity of the topological phase to variations of L_S is because this regime hosts spatially non-local MBSs, whose localization and zero-energy splitting strongly depends on L_S . In consequence, we can conclude that the nonreciprocity in the critical currents, and their

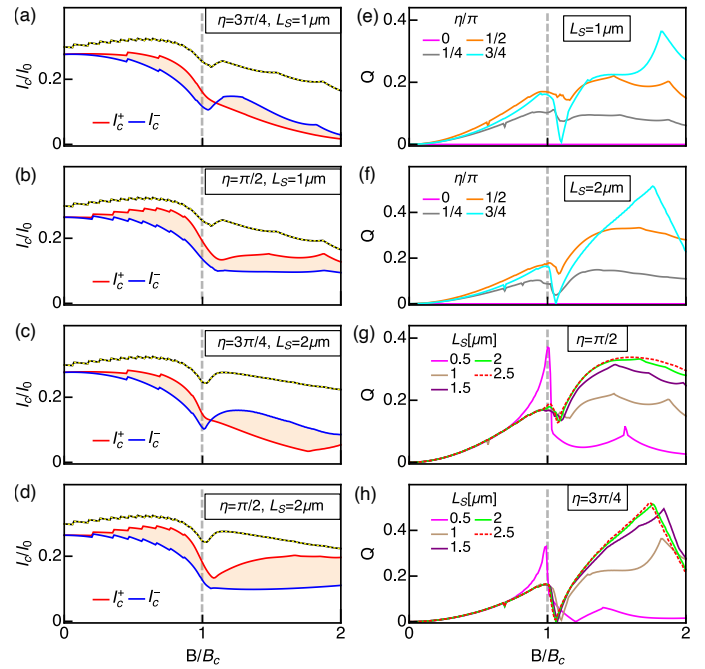


FIG. 4. Critical currents I_c^\pm (a-d) and quality factors Q (e-h) as a function of the Zeeman field B in S for different η and L_S . The black-yellow curve in (a-d) shows the critical current at $\eta = 0$ where there is no diode effect. The vertical dashed gray line marks the topological phase transition at $B = B_c$. Parameters: $L_N = 100\text{nm}$ and the rest as in Fig. 2.

JDs, gets enhanced entirely due to the presence of MBSs, specially, due to its spatial nonlocality.

The nonreciprocal critical currents discussed above give rise to quality factors Q with an interesting Zeeman dependence that confirms the crucial influence of the topological phase and its nonlocal MBSs [Fig. 4(e-h)]. At $\eta = 0$, the quality factor is zero because $I_c^+ = I_c^-$, as expected, see magenta lines in Fig. 4(e,f). In contrast, at $\eta \neq 0$, the quality factors Q acquire a strong dependence on B : Q gets finite values as B increases, reaching a pronounce feature at $B = B_c$ and finite values for $B > B_c$ that strongly depends on L_S [Fig. 4(e,f)] [82]. These features are absent in the trivial phase and, hence, suggest an intriguing effect due to MBSs. To support this view, in Fig. 4(g,h) we show Q as a function of B at $\eta = \pi/2, 3\pi/4$ and distinct L_S . The quality factors in the trivial phase do not respond to changes in L_S but they strongly react in the topological phase ($B > B_c$), giving rise to higher quality factors, see also [78]. The peak of Q at $B = B_c$ in Fig. 4(g,h) is due to the sharp Zeeman dependence of the ABS energies when the gap closing signals the topological phase transition. Since for $B > B_c$ the Majorana zero-energy splitting strongly depends on L_S , exhibiting vanishing values for long S regions, the response of the quality factors to changes in L_S seen in Fig. 4(g,h) is only attributed to the nonlocal MBSs. Thus, topological JJs can notably realize enhanced JDs, with larger quality

factors, due to the nonlocal nature of MBSs.

In conclusion, we studied the realization of Josephson diodes in finite topological Josephson junctions. We found that having a Zeeman field in the normal region parallel and perpendicular to the spin-orbit coupling induces Josephson diodes in the trivial and topological phases. We discovered that the quality factors of the Josephson diodes in the topological phase can be greatly enhanced entirely due to the spatial nonlocality of Majorana bound states. Similar Josephson junctions as those studied here based on superconductor-semiconductor hybrid systems have already been fabricated [14, 19, 36–38, 41, 42, 47], which places our findings within experimental reach. Our results thus establish topological superconductivity for realizing topological Josephson diodes with protected and superior functionalities.

We thank Y. Asano, S. Ikegaya, and S. Tamura for insightful discussions. J. C. acknowledges financial support from the Japan Society for the Promotion of Science via the International Research Fellow Program, the Swedish Research Council (Vetenskapsrådet Grant No. 2021-04121), and the Carl Trygger’s Foundation (Grant No. 22: 2093). N. N. acknowledges support from JST CREST Grant Number JPMJCR1874, Japan. Y. Tanaka acknowledges support from JSPS with Grants-in-Aid for Scientific Research (KAKENHI Grants No. 20H00131 and No. 23K17668).

-
- [1] L. A. Coldren, S. W. Corzine, and M. L. Mashanovitch, *Diode lasers and photonic integrated circuits* (John Wiley & Sons, 2012).
- [2] I. Mehdi, J. V. Siles, C. Lee, and E. Schlecht, THz diode technology: Status, prospects, and applications, *Proceedings of the IEEE* **105**, 990 (2017).
- [3] J. Semple, D. G. Georgiadou, G. Wyatt-Moon, G. Gelinck, and T. D. Anthopoulos, Flexible diodes for radio frequency (RF) electronics: a materials perspective, *Semicond. Sci. Technol.* **32**, 123002 (2017).
- [4] Y. Tokura and N. Nagaosa, Nonreciprocal responses from non-centrosymmetric quantum materials, *Nat. Commun.* **9**, 3740 (2018).
- [5] M. Kim, E. Pallecchi, R. Ge, X. Wu, G. Ducournau, J. C. Lee, H. Happy, and D. Akinwande, Analogue switches made from boron nitride monolayers for application in 5g and terahertz communication systems, *Nat. Electron.* **3**, 479 (2020).
- [6] K. Loganathan, H. Faber, E. Yengel, A. Seitkhan, A. Bakytbekov, E. Yarali, B. Adilbekova, A. AlBatati, Y. Lin, Z. Felemban, *et al.*, Rapid and up-scalable manufacturing of gigahertz nanogap diodes, *Nat. Commun.* **13**, 3260 (2022).
- [7] F. Braun, Ueber die stromleitung durch schwefelmetalle, *Ann. Phys.* **229**, 556 (1875).
- [8] S. M. Sze and M.-K. Lee, *Semiconductor devices: physics and technology* (Wiley, 2016).
- [9] F. Ando, Y. Miyasaka, T. Li, J. Ishizuka, T. Arakawa, Y. Shiota, T. Moriyama, Y. Yanase, and T. Ono, Observation of superconducting diode effect, *Nature* **584**, 373 (2020).
- [10] R. Wakatsuki, Y. Saito, S. Hoshino, Y. M. Itahashi, T. Ideue, M. Ezawa, Y. Iwasa, and N. Nagaosa, Nonreciprocal charge transport in noncentrosymmetric superconductors, *Sci. Adv.* **3**, e1602390 (2017).
- [11] S. Hoshino, R. Wakatsuki, K. Hamamoto, and N. Nagaosa, Nonreciprocal charge transport in two-dimensional noncentrosymmetric superconductors, *Phys. Rev. B* **98**, 054510 (2018).
- [12] K. Yasuda, H. Yasuda, T. Liang, R. Yoshimi, A. Tsukazaki, K. S. Takahashi, N. Nagaosa, M. Kawasaki, and Y. Tokura, Nonreciprocal charge transport at topological insulator/superconductor interface, *Nat. Commun.* **10**, 2734 (2019).
- [13] A. Daido, Y. Ikeda, and Y. Yanase, Intrinsic superconducting diode effect, *Phys. Rev. Lett.* **128**, 037001 (2022).
- [14] Y. Hou, F. Nichele, H. Chi, A. Lodesani, Y. Wu, M. F. Ritter, D. Z. Haxell, M. Davydova, S. Ilić, O. Glezakou-Elbert, A. Varambally, F. S. Bergeret, A. Kamra, L. Fu, P. A. Lee, and J. S. Moodera, Ubiquitous superconducting diode effect in superconductor thin films, *Phys. Rev. Lett.* **131**, 027001 (2023).
- [15] H. F. Legg, D. Loss, and J. Klinovaja, Superconducting diode effect due to magnetochiral anisotropy in topological insulators and rashba nanowires, *Phys. Rev. B* **106**, 104501 (2022).
- [16] J. J. He, Y. Tanaka, and N. Nagaosa, A phenomenological theory of superconductor diodes, *New J. Phys.* **24**, 053014 (2022).
- [17] N. F. Yuan and L. Fu, Supercurrent diode effect and finite-momentum superconductors, *Proc. Natl. Acad. Sci.* **119**, e2119548119 (2022).
- [18] H. Wu, Y. Wang, Y. Xu, P. K. Sivakumar, C. Pasco, U. Filippozzi, S. S. Parkin, Y.-J. Zeng, T. McQueen, and M. N. Ali, The field-free Josephson diode in a van der waals heterostructure, *Nature* **604**, 653 (2022).
- [19] C. Baumgartner, L. Fuchs, A. Costa, S. Reinhardt, S. Gronin, G. C. Gardner, T. Lindemann, M. J. Manfra, P. E. Faria Junior, D. Kochan, *et al.*, Supercurrent rectification and magnetochiral effects in symmetric Josephson junctions, *Nat. Nanotech.* **17**, 39 (2022).
- [20] B. Pal, A. Chakraborty, P. K. Sivakumar, M. Davydova, A. K. Gopi, A. K. Pandeya, J. A. Krieger, Y. Zhang, M. Date, S. Ju, *et al.*, Josephson diode effect from cooper pair momentum in a topological semimetal, *Nat. Phys.* **18**, 1228 (2022).
- [21] M. Davydova, S. Prembabu, and L. Fu, Universal Josephson diode effect, *Sci. Adv.* **8**, eabo0309 (2022).
- [22] K. K. Likharev, Superconducting weak links, *Rev. Mod. Phys.* **51**, 101 (1979).
- [23] M. Tinkham, *Introduction to superconductivity* (Courier Corporation, 2004).
- [24] I. Kulik and A. Omel’Yanchuk, Contribution to the microscopic theory of the Josephson effect in superconducting bridges, *JETP Lett.* **21**, 216 (1975).
- [25] A. Furusaki and M. Tsukada, Dc Josephson effect and Andreev reflection, *Solid State Commun.* **78**, 299 (1991).
- [26] A. Furusaki, H. Takayanagi, and M. Tsukada, Josephson effect of the superconducting quantum point contact, *Phys. Rev. B* **45**, 10563 (1992).
- [27] C. Beenakker, Three “universal” mesoscopic Josephson effects, in *Transport phenomena in mesoscopic systems: Proceedings of the 14th Taniguchi symposium, Shima,*

- Japan, November 10-14, 1991*, Vol. 109 (Springer-Verlag, 1992) p. 235.
- [28] A. Furusaki, Josephson current carried by Andreev levels in superconducting quantum point contacts, *Superlattices and Microstructures* **25**, 809 (1999).
- [29] S. Kashiwaya and Y. Tanaka, Tunnelling effects on surface bound states in unconventional superconductors, *Rep. Prog. Phys.* **63**, 1641 (2000).
- [30] Y. Asano, Direct-current Josephson effect in SNS junctions of anisotropic superconductors, *Phys. Rev. B* **64**, 224515 (2001).
- [31] Y. Asano, Y. Tanaka, and S. Kashiwaya, Anomalous Josephson effect in p -wave dirty junctions, *Phys. Rev. Lett.* **96**, 097007 (2006).
- [32] A. A. Golubov, M. Y. Kupriyanov, and E. Il'ichev, The current-phase relation in Josephson junctions, *Rev. Mod. Phys.* **76**, 411 (2004).
- [33] J. Sauls, Andreev bound states and their signatures, *Philos. Trans. Royal Soc. A* **376**, 20180140 (2018).
- [34] T. Mizushima and K. Machida, Multifaceted properties of andreev bound states: interplay of symmetry and topology, *Philos. Trans. R. Soc. A* **376**, 20150355 (2018).
- [35] Y. Tanaka, M. Sato, and N. Nagaosa, Symmetry and topology in superconductors—odd-frequency pairing and edge states—, *J. Phys. Soc. Japan* **81**, 011013 (2011).
- [36] J. Tiira, E. Strambini, M. Amado, S. Roddaro, P. San-Jose, R. Aguado, F. S. Bergeret, D. Ercolani, L. Sorba, and F. Giazotto, Magnetically-driven colossal supercurrent enhancement in inas nanowire Josephson junctions, *Nat. Commun.* **8**, 14984 (2017).
- [37] M. Hays, G. de Lange, K. Serniak, D. J. van Woerkom, D. Bouman, P. Krogstrup, J. Nygård, A. Geresdi, and M. H. Devoret, Direct microwave measurement of Andreev-bound-state dynamics in a semiconductor-nanowire Josephson junction, *Phys. Rev. Lett.* **121**, 047001 (2018).
- [38] L. Tosi, C. Metzger, M. F. Goffman, C. Urbina, H. Pothier, S. Park, A. L. Yeyati, J. Nygård, and P. Krogstrup, Spin-orbit splitting of andreev states revealed by microwave spectroscopy, *Phys. Rev. X* **9**, 011010 (2019).
- [39] H. Ren, F. Pientka, S. Hart, A. T. Pierce, M. Kosowsky, L. Lunczer, R. Schlereth, B. Scharf, E. M. Hankiewicz, L. W. Molenkamp, B. I. Halperin, and A. Yacoby, Topological superconductivity in a phase-controlled Josephson junction, *Nature* **569**, 93 (2019).
- [40] A. Fornieri, A. M. Whiticar, F. Setiawan, E. Portolés, A. C. C. Drachmann, A. Keselman, S. Gronin, C. Thomas, T. Wang, R. Kallaher, G. C. Gardner, E. Berg, M. J. Manfra, A. Stern, C. M. Marcus, and F. Nichele, Evidence of topological superconductivity in planar Josephson junctions, *Nature* **569**, 89 (2019).
- [41] F. Nichele, E. Portolés, A. Fornieri, A. M. Whiticar, A. C. C. Drachmann, S. Gronin, T. Wang, G. C. Gardner, C. Thomas, A. T. Hatke, M. J. Manfra, and C. M. Marcus, Relating Andreev bound states and supercurrents in hybrid Josephson junctions, *Phys. Rev. Lett.* **124**, 226801 (2020).
- [42] D. Razmadze, E. C. T. O'Farrell, P. Krogstrup, and C. M. Marcus, Quantum dot parity effects in trivial and topological Josephson junctions, *Phys. Rev. Lett.* **125**, 116803 (2020).
- [43] R. M. Lutchyn, E. P. Bakkers, L. P. Kouwenhoven, P. Krogstrup, C. M. Marcus, and Y. Oreg, Majorana zero modes in superconductor–semiconductor heterostructures, *Nat. Rev. Mater.* **3**, 52 (2018).
- [44] E. Prada, P. San-Jose, M. W. de Moor, A. Geresdi, E. J. Lee, J. Klinovaja, D. Loss, J. Nygård, R. Aguado, and L. P. Kouwenhoven, From andreev to majorana bound states in hybrid superconductor–semiconductor nanowires, *Nat. Rev. Phys.* **2**, 575 (2020).
- [45] S. M. Frolov, M. J. Manfra, and J. D. Sau, Topological superconductivity in hybrid devices, *Nat. Phys.* **16**, 718 (2020).
- [46] K. Flensberg, F. von Oppen, and A. Stern, Engineered platforms for topological superconductivity and majorana zero modes, *Nat. Rev. Mater.* **6**, 944 (2021).
- [47] G. P. Mazur, N. van Loo, D. van Driel, J. Y. Wang, G. Badawy, S. Gazibegovic, E. P. A. M. Bakkers, and L. P. Kouwenhoven, The gate-tunable Josephson diode, *arXiv:2211.14283* (2022).
- [48] X.-L. Qi and S.-C. Zhang, Topological insulators and superconductors, *Rev. Mod. Phys.* **83**, 1057 (2011).
- [49] M. Leijnse and K. Flensberg, Introduction to topological superconductivity and majorana fermions, *Semicond. Sci. Technol.* **27**, 124003 (2012).
- [50] C. Beenakker, Search for majorana fermions in superconductors, *Annu. Rev. Condens. Matter Phys.* **4**, 113 (2013).
- [51] M. Sato and Y. Ando, Topological superconductors: a review, *Rep. Prog. Phys.* **80**, 076501 (2017).
- [52] P. Marra, Majorana nanowires for topological quantum computation, *J. Appl. Phys.* **132**, 231101 (2022).
- [53] L. Fu and C. L. Kane, Superconducting proximity effect and majorana fermions at the surface of a topological insulator, *Phys. Rev. Lett.* **100**, 096407 (2008).
- [54] M. Sato, Y. Takahashi, and S. Fujimoto, Non-abelian topological order in s -wave superfluids of ultracold fermionic atoms, *Phys. Rev. Lett.* **103**, 020401 (2009).
- [55] Y. Tanaka, T. Yokoyama, and N. Nagaosa, Manipulation of the Majorana fermion, Andreev reflection, and Josephson current on topological insulators, *Phys. Rev. Lett.* **103**, 107002 (2009).
- [56] Y. Oreg, G. Refael, and F. von Oppen, Helical liquids and Majorana bound states in quantum wires, *Phys. Rev. Lett.* **105**, 177002 (2010).
- [57] R. M. Lutchyn, J. D. Sau, and S. Das Sarma, Majorana fermions and a topological phase transition in semiconductor-superconductor heterostructures, *Phys. Rev. Lett.* **105**, 077001 (2010).
- [58] P. San-Jose, E. Prada, and R. Aguado, ac Josephson effect in finite-length nanowire junctions with majorana modes, *Phys. Rev. Lett.* **108**, 257001 (2012).
- [59] J. Cayao, E. Prada, P. San-Jose, and R. Aguado, SNS junctions in nanowires with spin-orbit coupling: Role of confinement and helicity on the subgap spectrum, *Phys. Rev. B* **91**, 024514 (2015).
- [60] Y. Peng, F. Pientka, E. Berg, Y. Oreg, and F. von Oppen, Signatures of topological Josephson junctions, *Phys. Rev. B* **94**, 085409 (2016).
- [61] J. Cayao, P. San-Jose, A. M. Black-Schaffer, R. Aguado, and E. Prada, Majorana splitting from critical currents in Josephson junctions, *Phys. Rev. B* **96**, 205425 (2017).
- [62] J. Cayao, A. M. Black-Schaffer, E. Prada, and R. Aguado, Andreev spectrum and supercurrents in nanowire-based SNS junctions containing Majorana bound states, *Beilstein J. Nanotechnol.* **9**, 1339 (2018).
- [63] J. Cayao and A. M. Black-Schaffer, Distinguishing trivial and topological zero-energy states in long nanowire

- junctions, Phys. Rev. B **104**, L020501 (2021).
- [64] B. Pekerten, J. D. Pakizer, B. Hawn, and A. Matos-Abiague, Anisotropic topological superconductivity in Josephson junctions, Phys. Rev. B **105**, 054504 (2022).
- [65] L. Baldo, L. G. D. Da Silva, A. M. Black-Schaffer, and J. Cayao, Zero-frequency supercurrent susceptibility signatures of trivial and topological zero-energy states in nanowire junctions, Supercond. Sci. Technol. **36**, 034003 (2023).
- [66] S. D. Sarma, M. Freedman, and C. Nayak, Majorana zero modes and topological quantum computation, npj Quantum Inf. **1**, 15001 (2015).
- [67] V. Lahtinen and J. K. Pachos, A Short Introduction to Topological Quantum Computation, SciPost Phys. **3**, 021 (2017).
- [68] C. W. J. Beenakker, Search for non-Abelian Majorana braiding statistics in superconductors, SciPost Phys. Lect. Notes , 15 (2020).
- [69] R. Aguado and L. P. Kouwenhoven, Majorana qubits for topological quantum computing, Physics Today **73**, 44 (2020).
- [70] R. Aguado, A perspective on semiconductor-based superconducting qubits, Appl. Phys. Lett. **117**, 240501 (2020).
- [71] Y. Tanaka, B. Lu, and N. Nagaosa, Theory of giant diode effect in d -wave superconductor junctions on the surface of a topological insulator, Phys. Rev. B **106**, 214524 (2022).
- [72] P.-H. Fu, Y. Xu, C. H. Lee, S. A. Yang, Y. S. Ang, and J.-F. Liu, Field-effect Josephson diode via asymmetric spin-momentum locking states, arXiv:2212.01980 (2023).
- [73] H. F. Legg, K. Laubscher, D. Loss, and J. Klinovaja, Parity protected superconducting diode effect in topological Josephson junctions, arXiv:2301.13740 (2023).
- [74] B. Lu, S. Ikegaya, P. Buset, Y. Tanaka, and N. Nagaosa, Tunable Josephson diode effect on the surface of topological insulators, Phys. Rev. Lett. **131**, 096001 (2023).
- [75] J. J. Cuzzo, W. Pan, J. Shabani, and E. Rossi, Microwave-tunable diode effect in asymmetric squids with topological Josephson junctions, arXiv:2303.16931 (2023).
- [76] O. A. Awoga, J. Cayao, and A. M. Black-Schaffer, Supercurrent detection of topologically trivial zero-energy states in nanowire junctions, Phys. Rev. Lett. **123**, 117001 (2019).
- [77] T. Yokoyama, M. Eto, and Y. V. Nazarov, Anomalous Josephson effect induced by spin-orbit interaction and zeeman effect in semiconductor nanowires, Phys. Rev. B **89**, 195407 (2014).
- [78] See Supplemental Material at xxx for details.
- [79] J. Cayao and A. M. Black-Schaffer, Finite length effect on supercurrents between trivial and topological superconductors, Eur. Phys. J.: Spec. Top. **227**, 1387 (2018).
- [80] The finite current values at $\phi = 0$ when $\eta \neq 0$ suggest an intriguing relation between the so called ϕ_0 JJs and the asymmetric current-phase curves for $B > B_c$.
- [81] We note that I_c^\pm also develop very small kinks for $B > B_c$, but they are hard to see in [Fig. 4(a,b)] due to the small Majorana zero-energy splitting [Fig. 2(d)] as a result of having short S regions.
- [82] We stress that having $Q = 0$ at $B = 0$ is not a universal effect. In fact, we find that other L_N give finite Q already at $B = 0$ due to the combination of SOC and Zeeman field in N, see e.g., [78] for $L_N = 500\text{nm}$. In Ref. [78] we show that Q oscillates with L_N , reaching very small but finite values as L_N increases. We also note that Q can change sign for $B > B_c$ but find that it does not always happen for the same parameters, see cyan curve in Fig. 4(e,f) for $\eta = 3\pi/4$ and also Ref. [78].

Supplemental Material for “Enhancing the Josephson diode effect with Majorana bound states”

Jorge Cayao,¹ Naoto Nagaosa,² and Yukio Tanaka³

¹*Department of Physics and Astronomy, Uppsala University, Box 516, S-751 20 Uppsala, Sweden*

²*Center for Emergent Matter Science (CEMS), RIKEN, Wako, Saitama, 351-0198, Japan*

³*Department of Applied Physics, Nagoya University, Nagoya 464-8603, Japan*

(Dated: September 27, 2023)

In this supplemental material we provide further supporting the our findings of the main text. In particular, below we present additional calculations of the low-energy spectrum, critical currents, and quality factors for Josephson junctions (JJ) with distinct lengths of the normal (superconducting) region $L_{N(S)}$.

To begin, we remind that we here study finite superconductor-normal-superconductor (SNS) JJs with spin-orbit coupling (SOC) in the presence of Zeeman fields. The SOC is homogeneous all over the junction and oriented along y axis. In contrast, the Zeeman field is inhomogeneous: in the S regions it is along x and thus perpendicular to the SOC, but in the N region it has components that are parallel and perpendicular to the SOC. Thus, we denote the Zeeman field in S simply by B while in N it is given by $\mathbf{B}_N = B_N(\sin\theta \cos\eta, \sin\theta \sin\eta, \cos\theta)$, with $\theta \in (0, \pi)$ and $\eta \in (0, 2\pi)$. Thus, by taking $\theta = \pi/2$, η controls the Zeeman field in N to be either parallel or perpendicular to the SOC. As we discuss in the main text, having a Zeeman field parallel to the SOC creates an asymmetry in the Andreev spectrum that turns out to be essential ingredient for producing Josephson diodes in JJs. Below we provide further calculations supporting the realization of Josephson diodes in the presence of Majorana bound states (MBSs)

CRITICAL CURRENTS AND QUALITY FACTORS FOR VERY SHORT N REGIONS

In this section we focus on JJs with middle N regions having $L_N = 20\text{nm}$. Before going further, we point out that the Andreev spectrum of these very short JJs was presented in Fig. 1(a,b) of the main text. Here, we provide further details on the critical currents I_c^\pm and quality factors Q . This is presented in Fig. S1 as a function of the Zeeman field B for different values of η , which characterizes the orientation of the Zeeman field in N. For comparison, we also show the critical currents at $\eta = 0$, see dashed black-yellow curve.

As the Zeeman field B increases, the critical currents I_c^\pm first decrease and develop a kink at the topological phase transition $B = B_c$, see Fig. S1(a,b). Above B_c , the critical currents develop oscillations which stem from the Majorana zero-energy splitting seen in the Andreev spectrum. Such critical current oscillations are washed out when the S regions become longer Fig. S1(c,d), and property that reflects the spatial nonlocality of MBS. We note that both critical currents I_c^\pm exhibit roughly the same behaviour, with very small deviations at strong B , close to and in the topological phase. As we discussed in the main text, these small deviations signal the occurrence of the Josephson diode effect. To characterize the diode effect, in Fig. S1(e-h) we show the quality factors as a function of the Zeeman field B as $Q = |I_c^+ - I_c^-| / (I_c^+ + I_c^-)$. Here we can observe that the deviations in the critical currents I_c^\pm produce finite quality factors, which are highly dependent on the orientation of the Zeeman field in N.

An intriguing result in this part is that the quality factors strongly depend on the length of the S regions L_S in the topological phase ($B > B_c$) but do not in the trivial phase ($B < B_c$). Interestingly, by increasing the length of S in the topological phase, the quality factors acquire larger values and saturate to a finite value when the four MBSs are truly zero modes, see Fig. S1(g,h). In the trivial phase, in contrast, the quality factors do not change when L_S varies. As explained in the main text, this effect stems from the fact that only the topological phase hosts nonlocal states, the MBSs, which are located at the ends of the S regions and therefore depend on the length of the S regions L_S . This length dependence in the topological phase forces the zero-energy Majorana splitting seen in the spectrum in Fig. 1(a,b) to reach zero energy for long S regions, which then gives rise to larger quality factors. Furthermore, it is worth noting that the quality factors here are smaller than for the JJs with $L_N = 100\text{nm}$ shown in Fig. 4 of the main text. Nevertheless, the positive impact of MBSs, that they increase the quality factors in the topological phase, remains, thus supporting our findings of the main text.

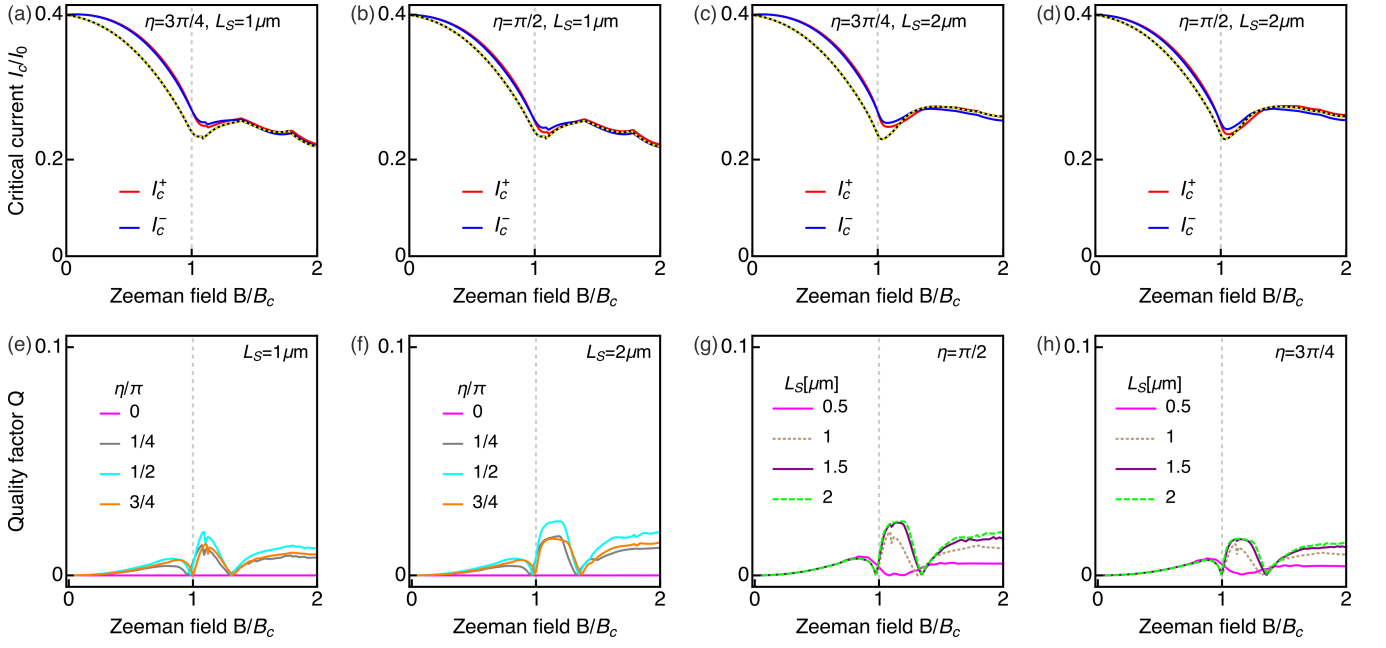


FIG. S1. Critical currents I_c^{\pm} (a-d) and quality factors Q (e-h) as a function of the Zeeman field B in Josephson junctions with $L_N = 20\text{nm}$ for different η and L_S . The black-yellow curve in (a-d) shows the critical current at $\eta = 0$ where there is no diode effect. The vertical dashed gray line marks the topological phase transition at $B = B_c$. Parameters: $\alpha = 40\text{meVnm}$, $\mu = 0.5\text{meV}$, $\theta = \pi/2$, $\Delta = 0.5\text{meV}$, $B_N = 0.5\text{meV}$, $I_0 = e\Delta/\hbar$.

ANDREEV SPECTRUM, CRITICAL CURRENTS, AND QUALITY FACTORS FOR N REGIONS WITH INTERMEDIATE LENGTHS

In this section we focus on JJs with middle N regions having $L_N = 500\text{nm}$. First, in Fig. S2 we show the low-energy spectrum as a function of the phase difference ϕ in the trivial ($B = 0.5B_c$) and topological phases ($B = 1.5B_c$) and different η and L_S . Then, in Fig. S3 we present the critical currents I_c^{\pm} and quality factors Q as a function of the Zeeman field B for different η and L_S .

With respect to the phase-dependent Andreev spectrum, the first observation is that it does not depend on the length of the S regions L_S in the trivial phase, see top row of Fig. S2; the only effect of L_S in this regime is that it adds more levels to the quasicontinuum, which is above the induced gap. The spectrum, however, depends on the orientation of the Zeeman field in N, via η and seen, for instance, by comparing panels (a,c) with (b,d). This dependence induces an asymmetry around $\phi = \pi$ in both the ingap Andreev bound states and the quasicontinuum above the induced gap. In the topological phase, however, the situation is different, see bottom row of Fig. S2. While short S regions develop a finite Majorana zero-energy splitting, such zero-energy splitting is considerably reduced in long S regions, leading to MBSs with zero energy, see Fig. S2(e-h) and vertical dashed red lines. This dependence on the length of the S regions stems from the fact that the topological regime hosts spatially localized MBSs, as discussed in previous section and also in the main text. Furthermore, we note that, besides the effect of L_S , the spectrum in the topological phase also depends on the orientation of the Zeeman field in N. It becomes asymmetric with respect to $\phi = \pi$, and has regimes with the Majorana zero-energy splitting away from π . In sum, the spectrum in the trivial phase does not depend on L_S but, interestingly, the Andreev spectrum in the topological phase, accompanied by the Majorana zero-energy splitting, strongly depend on the length of the S regions.

The properties of the Andreev spectrum determine the profile of the critical currents I_c^{\pm} and quality factors Q , as we can see in Fig. S3. The very first feature in the critical currents is that a $\eta \neq 0$ induces $I_c^+ \neq I_c^-$, which can be clearly seen in the orange region between blue and red curves. This feature shows the emergence of the Josephson diode effect. Note that at $\eta = 3\pi/4$, the JJ exhibits a diode effect already at $B = 0$, which persists even for $B > B_c$ but with a reduced size in short S regions [Fig. S3(a)]. The critical currents I_c^{\pm} also develop oscillations above B_c , which occurs due to the Majorana zero-energy splitting revealed in the phase-dependent spectrum [Fig. S2(e,f)]; At $\eta = 0$, both I_c^{\pm} exhibit the same behaviour as a function of B , see black-yellow dashed curves. Moreover, for $\eta = \pi/2$ the considered JJ at $B = 0$ has $I_c^+ = I_c^-$ and thus no sign of a diode effect but at large B the JJ realizes $I_c^+ \neq I_c^-$,

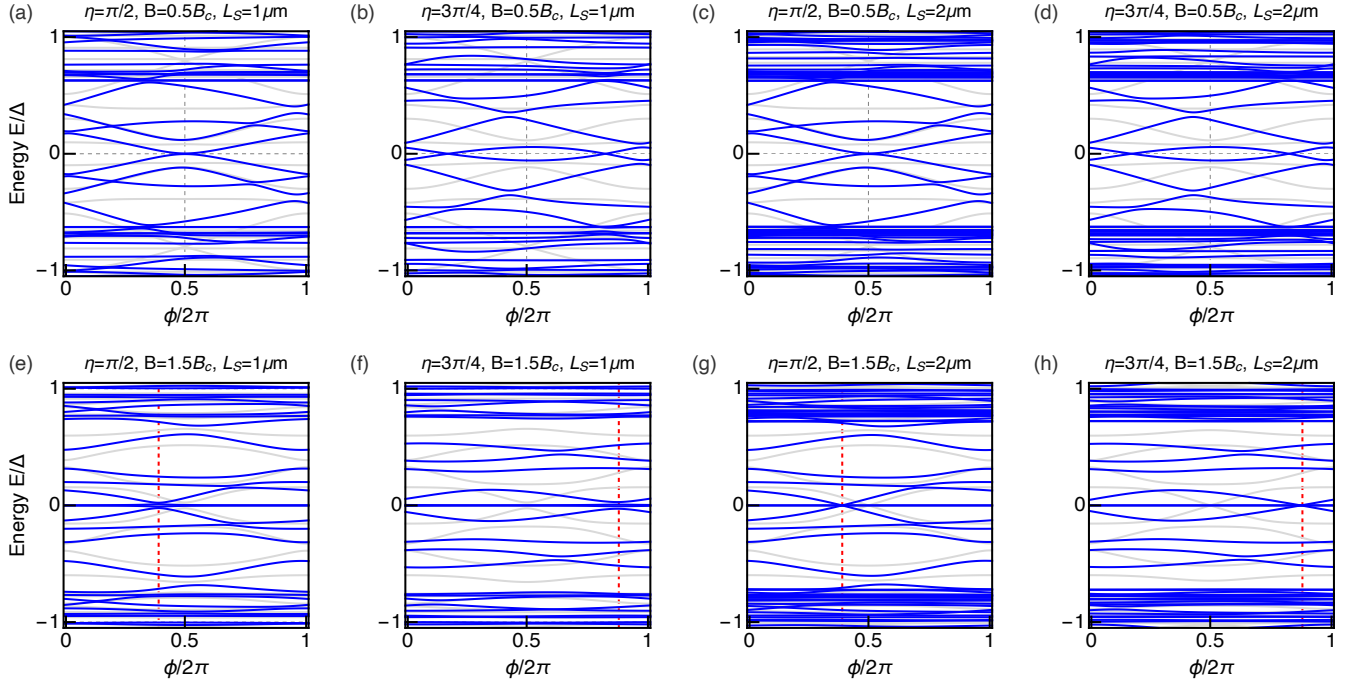


FIG. S2. Low-energy spectrum as a function of ϕ in Josephson junctions with $L_N = 500\text{nm}$ and different η in the trivial (a-d) and topological (e-h) phases. Gray curves in all panels correspond to $\eta = 0$. Vertical dashed lines mark where four MBSs appear and their zero-energy splitting. Parameters: $\alpha = 40\text{meVnm}$, $\mu = 0.5\text{meV}$, $\theta = \pi/2$, $\Delta = 0.5\text{meV}$, $B_N = 0.5\text{meV}$.

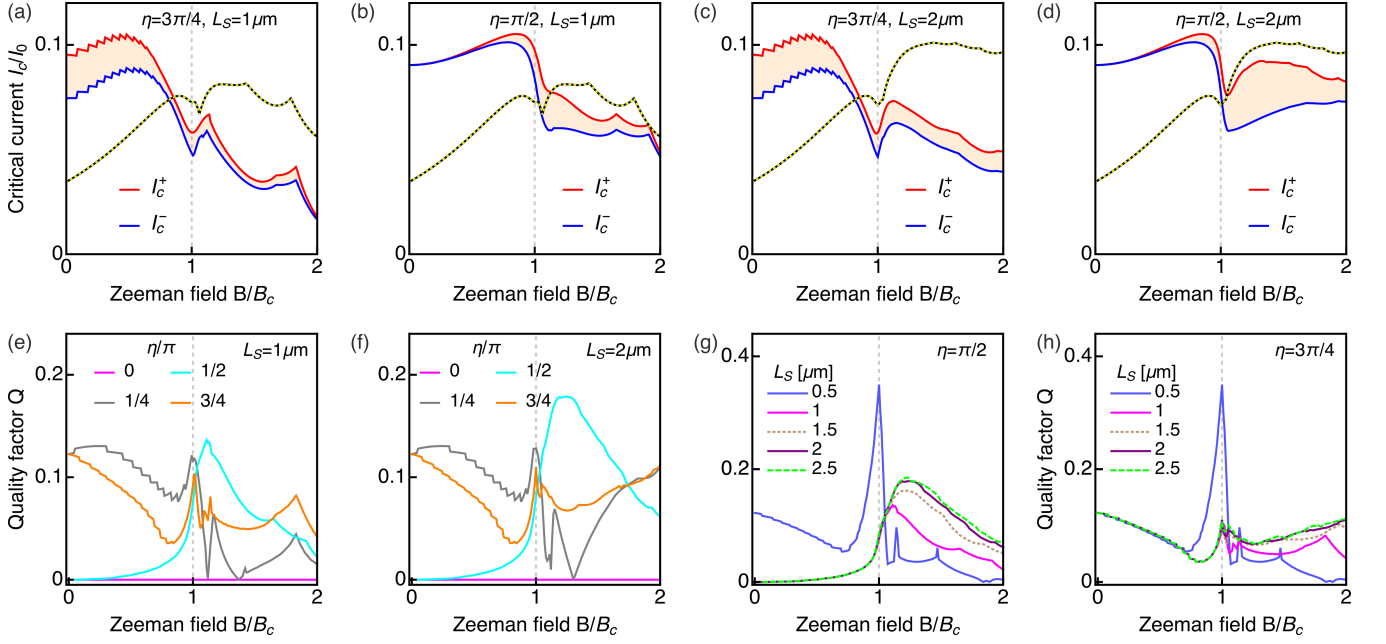


FIG. S3. Critical currents I_c^\pm (a-d) and quality factors Q (e-h) as a function of the Zeeman field B in Josephson junctions with $L_N = 500\text{nm}$ for different η and L_S . The black-yellow curve in (a-d) shows the critical current at $\eta = 0$ where there is no diode effect. The vertical dashed gray line marks the topological phase transition at $B = B_c$. Parameters: $\alpha = 40\text{meVnm}$, $\mu = 0.5\text{meV}$, $\theta = \pi/2$, $\Delta = 0.5\text{meV}$, $B_N = 0.5\text{meV}$, $I_0 = e\Delta/\hbar$.

which, interestingly, induces a finite diode effect [Fig. S3(b)]. Larger S regions gives a larger difference between I_c^+ and I_c^- , which can be seen to produce a larger Josephson diode effect [Fig. S3(c,d)]. As discussed in the main text, the dependence of the critical currents on L_S in the topological phase is due to the presence of MBSs.

The Josephson diode effect can be further seen in their quality factors, presented in the bottom row of Fig. S3. As expected due to the discussion in previous paragraph, the regime with $\eta = 3\pi/4$ exhibits a finite quality factor already at $B = 0$ diode effect, which persists at finite B and even reveal the Majorana oscillations in the topological phase. At $\eta = \pi/2$ a finite quality factor appears at strong B as B approaches the topological phase transition at B_c : It develops a maximum after B_c and also reflects the Majorana oscillations for $B > B_c$, see cyan curves in Fig. S3(e,f). Note that these quality factors are smaller than those found for $L_N = 100\text{nm}$, showing the dependence of the diode effect on L_N . By exploring the dependence on L_S we find that the quality factors in the topological phase get considerably enhanced as L_S increases Fig. S3(g,h), effect that can be only attributed to the presence of MBSs. This, again, supports our main finding, that MBSs enhance the Josephson diode effect, discussed in the main text.

IMPACT OF THE LENGTH OF THE S AND N REGIONS ON THE QUALITY FACTORS

In this section we analyze the dependence of the quality factors Q on L_S and L_N . In particular, in Fig. S4 we show the quality factors in the trivial and topological regimes as a function of L_S and L_N for $\eta = \pi/2, 3\pi/4$. We consider two characteristic values of the Zeeman field for the trivial ($B = 0.5B_c$) and topological ($B = 1.5B_c$) phases but our conclusions are valid for all B in such trivial and topological regimes.

In the trivial phase ($B < B_c$), the quality factors do not depend on L_S , see magenta curves in Fig. S4(a-f), irrespective of the length of the N region and the value of η . As exposed in previous sections and also in the main text, this occurs because the trivial regime does not host spatially nonlocal states. In contrast, in the topological phase ($B > B_c$) the quality factors are affected by L_S : they increase as L_S acquires larger values and saturate when the four MBSs acquire zero energy, see brown curves in in Fig. S4(a-f). This therefore makes MBSs to be important for enhancing the Josephson diode effect in finite topological JJs. Furthermore, we note that the quality factors exhibit an oscillatory behaviour as a function of L_N in both the trivial and topological phases; for relatively short N regions, however, the quality factors in the topological phase can reach higher values than those in the trivial phase. In sum, we find that the spatial nonlocality of MBSs plays a key role for enhancing the Josephson diode effect, as argued in the main text.

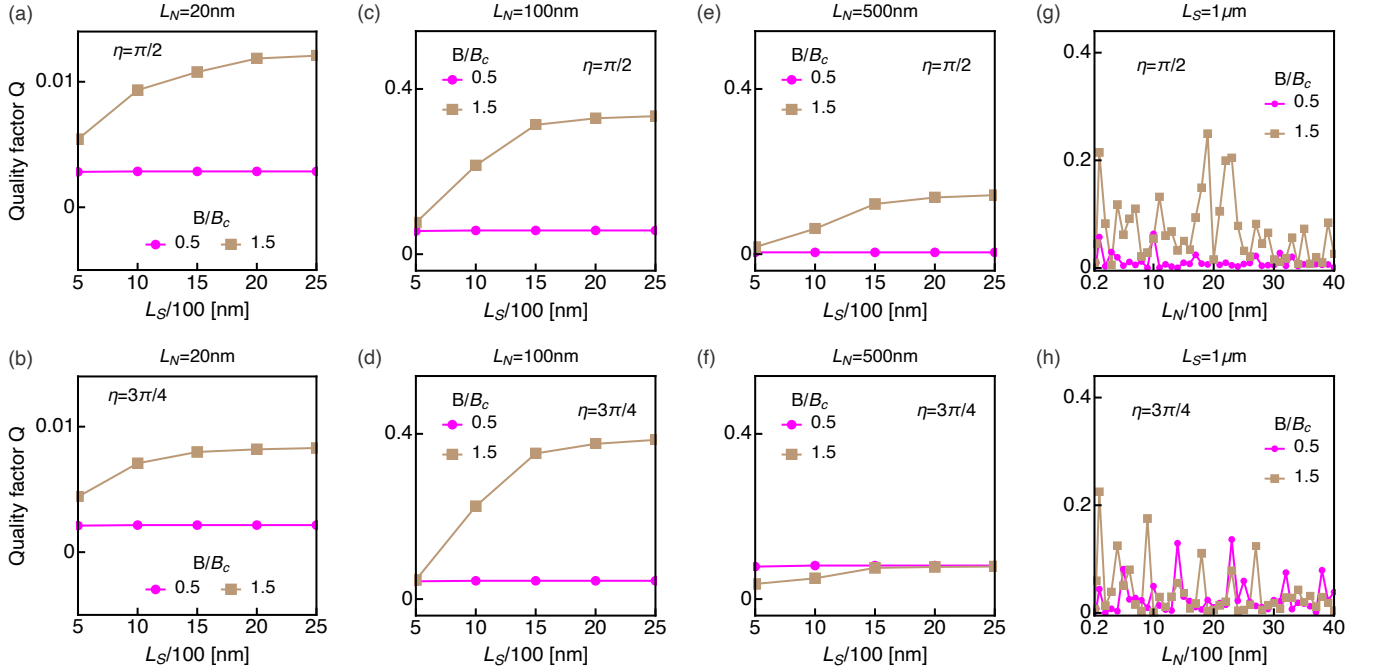


FIG. S4. Critical currents as a function of L_S (a-f) and as a function of L_N (g,h) in the trivial ($B < B_c$) and topological phases ($B > B_c$) for $\eta = \pi/2, 3\pi/4$. Parameters: $\alpha = 40\text{meVnm}$, $\mu = 0.5\text{meV}$, $\theta = \pi/2$, $\Delta = 0.5\text{meV}$, $B_N = 0.5\text{meV}$, $I_0 = e\Delta/\hbar$.